J Mater Sci: Mater Electron (2023) 34:1051

Dielectric and energy storage properties of $Ba_{0.85}Ca_{0.15}Zr_{0.1}Ti_{0.90}O_3$ ceramics with $BaO–Na_2O–Nb_2O_5–WO_3–P_2O_5$ glass addition

A. Ihyadn[1,*], S. Merselmiz[1], D. Mezzane[1,2], L. Bih[3], A. Lahmar[2], A. Alimoussa[1], M. Amjoud[1], Igor A. Luk'yanchuk[2,4], and M. El Marssi[2]

[1] *IMAD-Lab, Cadi Ayyad University, Avenue Abdelkrim El Khattabi, P.B. 549, 40000 Marrakesh, Morocco*
[2] *Condensed Matter Physics Laboratory, University of Picardie Jules Verne, Amiens, France*
[3] *Laboratoire Des Sciences Et Métiers de L'ingénieur (LSMI), ENSAM Meknès, Université Moulay Ismail, Meknès, Morocco*
[4] *Department of Building Materials, Kyiv National University of Construction and Architecture, Kyiv 03680, Ukraine*

Received: 16 March 2023
Accepted: 17 April 2023
Published online:
27 April 2023

ABSTRACT

Lead-free $Ba_{0.85}Ca_{0.15}Zr_{0.10}Ti_{0.90}O_3$ (BCZT) ceramic with different $BaO–Na_2O–Nb_2O_5–WO_3–P_2O_5$ (BNNWP) glass contents, forming (1–*x*)BCZT–*x*BNNWP lead-free ceramics (abbreviated as BCZT*x*; *x* = 0, 2, 4, 6, and 8wt%) were synthesized using the conventional solid-state processing route. The XRD investigation shows the coexistence of tetragonal and orthorhombic phases in BCZT pure. Likewise, only the tetragonal phase was detected in BCZTx (*x* = 2–8 wt%) ceramics. The SEM findings indicate that the average grain size decreases as the amount of BNNWP glass additives increases. In addition, BCZT ceramics modified with glass additions showed narrower hysteresis loops and a large electric field. The BCZT4 showed the highest recovered energy density of 0.52 J/cm^3 at 135 kV/cm with an energy storage efficiency of 62.4%, which is increased by 6.6 compared to BCZT0 (0.075 J/cm^3). The energy density was also calculated using the Landau–Ginzburg–Devonshire (LGD) theory.

1 Introduction

Pulse power technology has found significant application in electron beam, nuclear technologies, hybrid electric cars, and medical defibrillators. As a result of fast industrial development, it has continuously progressed into industrial and civil fields [1, 2]. Capacitors with higher storage density, faster charge–discharge rate, higher breakdown strength (BDS), and better thermal stability are required in modern electrical and electronic equipment [3, 4]. The fundamental obstacle to their use in electrical and high power systems is their poor energy density [5, 6]. The energy storage density is affected by the material's dielectric constant and the electrical breakdown resistance [7, 8]. Dielectric ceramics have a comparatively high dielectric constant and a low breakdown

Address correspondence to E-mail: ihyadn.abderrahim@gmail.com

https://doi.org/10.1007/s10854-023-10483-x

strength when compared to other energy storage materials [3, 9].

Dielectric materials based on $BaTiO_3$ have been widely investigated for energy storage systems due to their high constant dielectric and low dielectric loss [10–13]. Numerous recent research have discussed the impact of Ca^{2+} and Zr^{4+} substituting for Ba^{2+} and Ti^{4+} in $BaTiO_3$ ceramics to form $Ba_{0.85}Ca_{0.15}Zr_{0.10}Ti_{0.90}O_3$ (BCZT) ceramic. The results show that BCZT shows interesting piezoelectric and dielectric properties due to the closeness to morphotropic phase boundary (MPB) [14–16]. Unfortunately, pure BCZT ceramic displays low breakdown strength and low energy efficiency, resulting in poor energy storage properties and restricting its usage as an energy storage device. Hence, numerous researchers have developed several methods to enhance the BDS of ceramics in order to ensure sufficient energy storage performances [17–19]. The findings reveal that these drawbacks can be overcome by modifying the microstructure and the chemical composition of the ceramics. For instance, by adding additives like oxides and glasses to the dielectric ceramics one can considerably hence the breakdown strength (BDS) and hence improve the energy efficiency [4, 9, 20]. The addition of glass can significantly increase the breakdown resistance of dielectric ceramics. An appropriate amount of glass liquid phase will promote the rearrangement of grain microstructure, decreasing the sintering temperature and densifying the ceramics [4, 21].

Recent literature investigations found that BCZT ceramics modified by glass addition presents improved energy storage and BDS. Among various reported glass systems, B_2O_3–SiO_2-based glasses such as B_2O_3–Al_2O_3–SiO_2, Bi_2O_3–B_2O_3–SiO_2, and BaO–B_2O_3–ZnO present the particular interest [2, 22, 23]. The BDS of BCZT ceramics with glass additions was greatly improved by decreasing the grain size and densifying the microstructure [2, 22]. However, a little number of researches was allocated to use phosphate glass with a low melting temperature compared to the SiO_2 and B_2O_3 glasses [24, 25]. In addition, phosphate glasses exhibit a simple composition and good glass-forming ability [26].

In this work, $Ba_{0.85}Ca_{0.15}Zr_{0.10}Ti_{0.90}O_3$ (BCZT) ceramics with phosphate glass BaO–Na_2O–Nb_2O_5–WO_3–P_2O_5 (BNNWP) addition were synthesized using the conventional solid-state technique. The effect of BNNWP glass addition on dielectric and energy storage performances of BCZT ceramics was studied. The main objective is to obtain (1–*x*)BCZT–*x*BNNWP ceramics with enhanced energy storage properties. Furthermore, the energy storage densities were calculated using the Landau–Ginzburg–Devonshire (LGD) phenomenological theory. The modeling result confirms the experimental finding for $BaTiO_3$–$BaSnO_3$ as described by Yao et al. [27].

2 Experimental procedure

2.1 Synthesis of (1–*x*)BCZT–*x*BNNWP ceramics

A series of (1–*x*)BCZT–*x*BNNWP ceramics (*BCZTx*, *x* = 0, 2, 4, 6, and 8wt%) designated as BCZT0, BCZT2, BCZT4, BCZT6, BCZT8 were synthesized via the conventional solid-state technique. Meanwhile, BCZT powders and BaO–Na_2O–Nb_2O_5–WO_3–P_2O_5 glass were prepared according to our previous works [16, 26]. For BCZT*x* formation, both powders were weighed according to the nominally (1-*x*) BCZT–xBNNWP composition and then milled in an agate mortar with ethanol. Subsequently, the obtained powders were formed into 13 mm discs and sintered in air for 7 h at temperatures between 1300 and 1250 °C. The BCZT*x* ceramics were sintered at temperatures with the highest bulk density. The appropriate sintering temperature corresponds to the highest density and the value is 1350 °C, 1300 °C, 1275 °C, 1250 °C, and 1250, respectively, when *x* = 0, 2, 4, 6, and 8wt%.

2.2 Characterizations

The phase structure of BCZT*x* ceramics was analyzed by the X-ray diffraction(XRD, Panalytical™ X-Pert Pro spectrometer) using CuK_α radiation ($\lambda \sim 1.5406$ Å). The density (d) of the BCZT*x* was measured at room temperature by Archimedes method. Scanning electron microscope (SEM, Tescan VEGA3) was used to examine the morphology of BCZT*x* ceramics. For electrical measurements, sintered ceramics coated with a silver paste form electrodes. The dielectric properties were measured by using an impedance analyzer (LCR meter hp 4284A 20 Hz-1 MHz). The polarization–electric field (*P*–*E*) hysteresis loops of a BCZT*x* ceramics with a thickness of 0.25 mm were investigated with the CPE1701,

PolyK, USA, with a high voltage power supply (Trek 609-6, USA).

3 Results and discussions

3.1 Phase structure evolution

Figure 1 depicts the XRD patterns of BCZTx ceramics. The prepared ceramic BCZT0 reveals the coexistence of tetragonal (T) and orthorhombic (O) phases. The splitting of the peaks at $2\theta \approx 44$–$46°$ confirms the quadratic phase's existence [16, 28]. Moreover, the formation of the BCZT sample at the Morphotropic Phase Boundary (MPB) is evidenced by the presence of the triplet $(022)_O/(200)_T/(200)_O$ around $2\theta \approx 45°$ as reported in our previous work [16]. However, the MPB disappears after the BNNWP glass addition. BCZT glass-modified only shows the existence of tetragonal phase. This indicates that combining the glass phase with the BCZT structure results in the formation of the tetragonal phase instead of the coexisting of two phases (O and T). It seems that the introduction of the glass inhibits the crystal growth of the orthorhombic structure and promotes the transformation of the O phase into the more stable T phase. Additionally, the peak intensity of secondary phases (α) increases as the glass content rises.

3.2 Microstructure analysis and density

Figure 2 illustrates SEM micrographs of BCZTx ceramics. The inclusion of small amounts of BNNWP glass reduces the average grain size of BCZTx ceramics. It decreases from 6.4 to 1.25 µm when x increases from 0 to 8wt%. This decrease could be attributed to the BNNWP liquid glass phase acting as an inhibitor of grain growth and grain boundary migration [2, 21, 29]. In addition, this reduction in grain size could be beneficial in increasing the compactness of ceramics. Moreover, the fine grain size and highest density could improve the breakdown strength, required for high-energy storage density [4, 9]. Accordingly, the addition of glass enhances the densification of BCZTx ceramics, as shown in Fig. 3. The liquid BNNWP glass at high temperature decreases the sintering temperature and increases the density of BCZTx ceramics. The average relative density of samples is between 93 and 97% of the theoretical maximum density, indicating the improvement of the material density and the reduction of pores.

3.3 Dielectric properties

Figure 4 displays the temperature dependency of the dielectric constant (ε_r) of BCZTx ceramics at various frequencies. Table 1 provides the dielectric properties obtained for all the ceramics. BCZTx ceramics exhibit two distinct polymorphic phase transitions that correspond to the orthorhombic–tetragonal (O–T) and

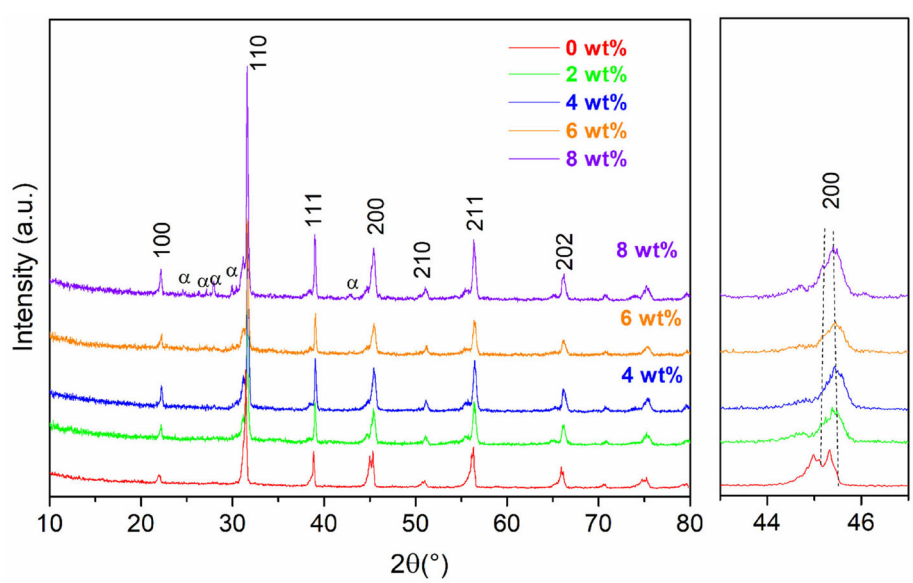

Fig. 1 XRD patterns of BCZTx ceramics

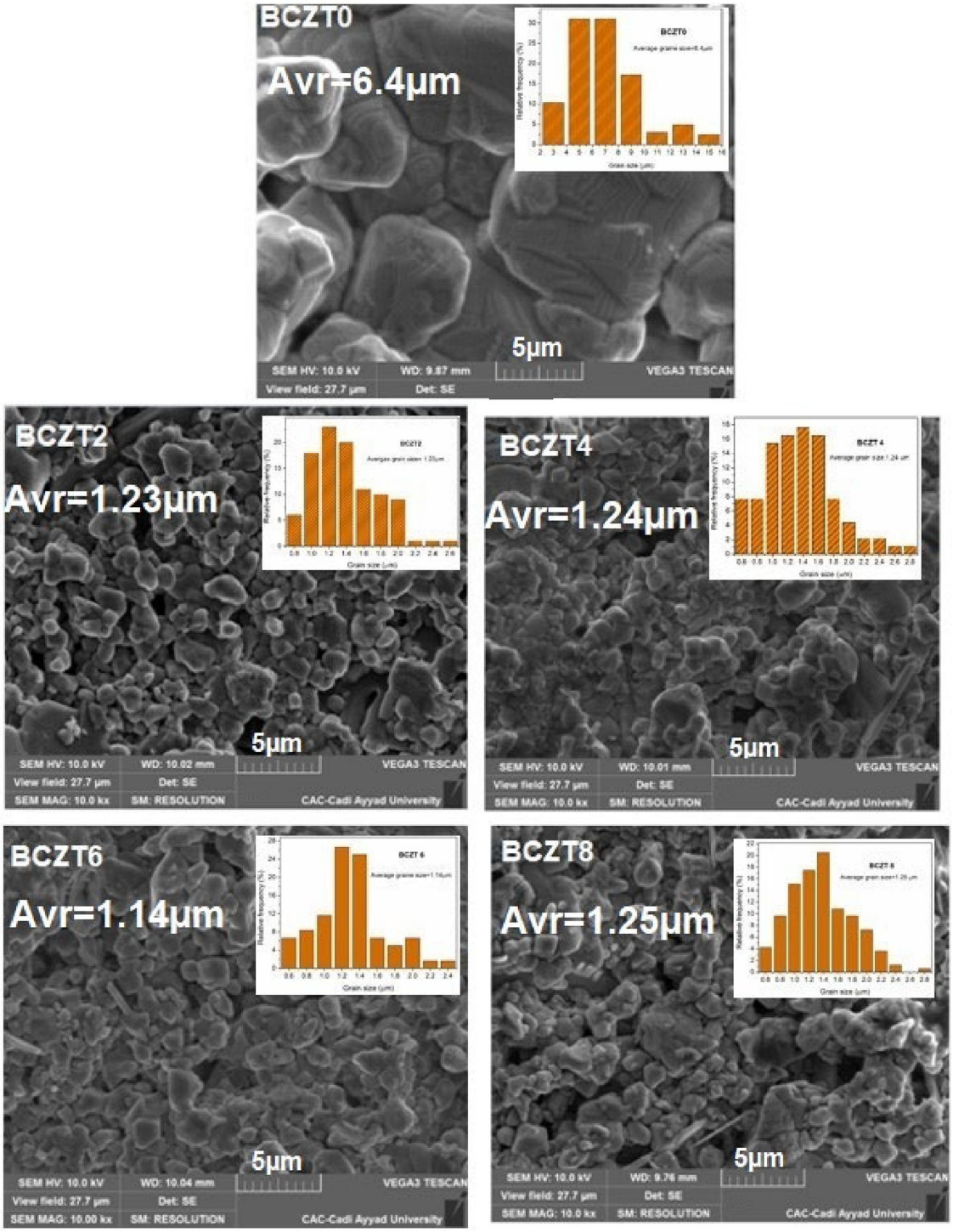

Fig. 2 SEM images of BCZT*x* ceramics

tetragonal–cubic (T–C) transitions. The dielectric peak temperature of the O–T phase transition ($T_{O\text{-}T}$) is about 35.0, 24.7, 22.3, 23.4, and 29.5 °C for BCZT0, BCZT2, BCZT4, BCZT6, and BCZT8 ceramics, respectively. In addition, the Curie temperature (T_c) depends significantly on the glass content. The T_c drops from 92 to 63 and then increases to 86, 84, 80 °C as the glass content rises from 0 to 2, 4, 6, and 8 wt%, respectively. The drop in Tc may be ascribed to the transition from a long-term to a short-term order [30],

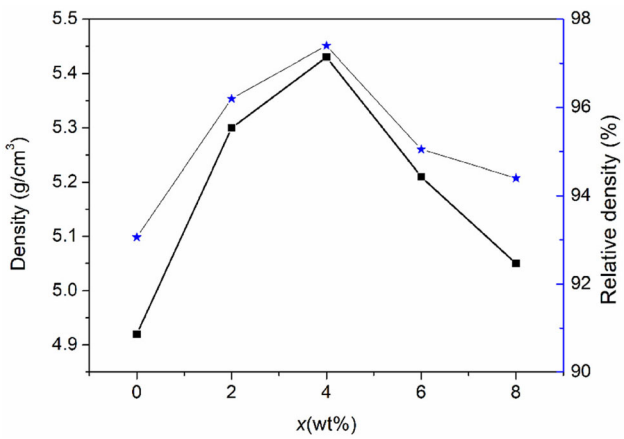

Fig. 3 Density of BCZTx ceramics

which promotes the generation of polar nanoregions (PNRs) [31] and the internal clamping originating from the existence of an immobile non-ferroelectric glass phase[32]. For instance, the value of the ε_r at T_c decreases significantly from 5400 for BCZT0 to 524 for BCZT8 with increasing BNNWP glass ratio. In addition, Table 1 indicates that the difference between ε_m (1 kHz, Tc) and ε_r (1 kHz, 30 °C) for BCZT ceramics decreases with increasing glass addition. Hence, introducing the BNNWP glass phase improves the thermal stability of the dielectric constant which is advantageous for capacitor materials[33]. The temperature dependence of the dielectric constant (ε_r) of BCZTx ceramics at 1 kHz is illustrated in Fig. 5. In addition, it is noticed that the dielectric constant decreases gradually as the glass content increases and the dielectric temperature curves of BCTZ4 and BCTZ6 are almost coincided. For instance, the dielectric constant of the pure BCZT drops significantly from 2640 to 1587, 692, 630, and 488 for BCZT2, BCZT4, and BCZT8, respectively. This behavior is associated with the dilution of the low ε_r of BNNWP glass (ε_r = 34) [22, 29]. In addition, this decrease could be attributed to the ceramic's grain size reduction. It has been stated that smaller ceramic grain size leads to a lower dielectric constant [4, 34]. Moreover, the similarity of the dielectric temperature curves of BCTZ4 and BCTZ6 could be attributed to the formation of similar bond defects and the heterogeneous phase within these samples.

Figure 6 depicts the temperature dependence of the dielectric losses (tan δ) of BCZTx ceramics at 1 kHz. A significant increase in *tanδ* is observed near the O–T phase transition. This could be associated with the increase in conductivity, the internal stress, and space charge caused by the interface of BCZT and glass phase [35]. Note that except for the BCZT2 composition, a small increase of *tan δ* is noted beyond 40 °C. However, the values of the dielectric losses are still low (< 0.15).

Figure 7 shows the frequency dependence of ε_r and *tanδ* of BCZTx ceramics at room temperature. The frequency evolution of ε_r reveals excellent dielectric stability for all compositions except BCZT0 and BCZT8. Furthermore, *tanδ* decreases with increasing the frequency in the range of 100 Hz-10 kHz. However, the evolution of *tanδ* remains stable in the frequency range of 10 kHz-1 MHz. It is worth noting that this result is beneficial for ceramics used in electrical energy storage [22, 33].

3.4 Energy storage performances

Figure 8a–e illustrates the room temperature electric field dependence of the *P–E* hysteresis loops of BCZTx ceramics at 100 Hz. It is evident that BCZT ceramics display typical ferroelectric behavior. Additionally, the hysteresis loops get thinner and the applied electric field increases as the glass content increases. Furthermore, under the same electric field, the polarization of the modified BCZTx ceramics is less than that BCZT0 because of the added BNNWP glass's low permittivity, as indicated by the dielectric constant characteristics. Figure 8f displays the variation of the maximum polarization (P_{max}), remnant polarization (P_r), and the maximal electric field (E_{max}) of BCZTx ceramics. It is noted that the P_{max} and E_{max} values of BCZTx ceramics increase to a maximum and then decrease as the glass content increases. Besides, P_r value decreases steadily as glass content increases. It is worthy to mention that the remnant polarization of the ceramics coincides to the dielectric constant's variation. (Fig. 5). Despite the fact that the dielectric characteristics deteriorate when more glass is added, the drop in P_r is critical for improving energy storage density. This drop could be ascribed to the formation of polar nanoregions (PNRs) as observed in the behavior of the decrease of Tc. PNRs have lower energy barriers and better thermal stability than typical ferroelectric domains, yielding in thin *P–E* hysteresis loops with low P_r and high breakdown strength [31].

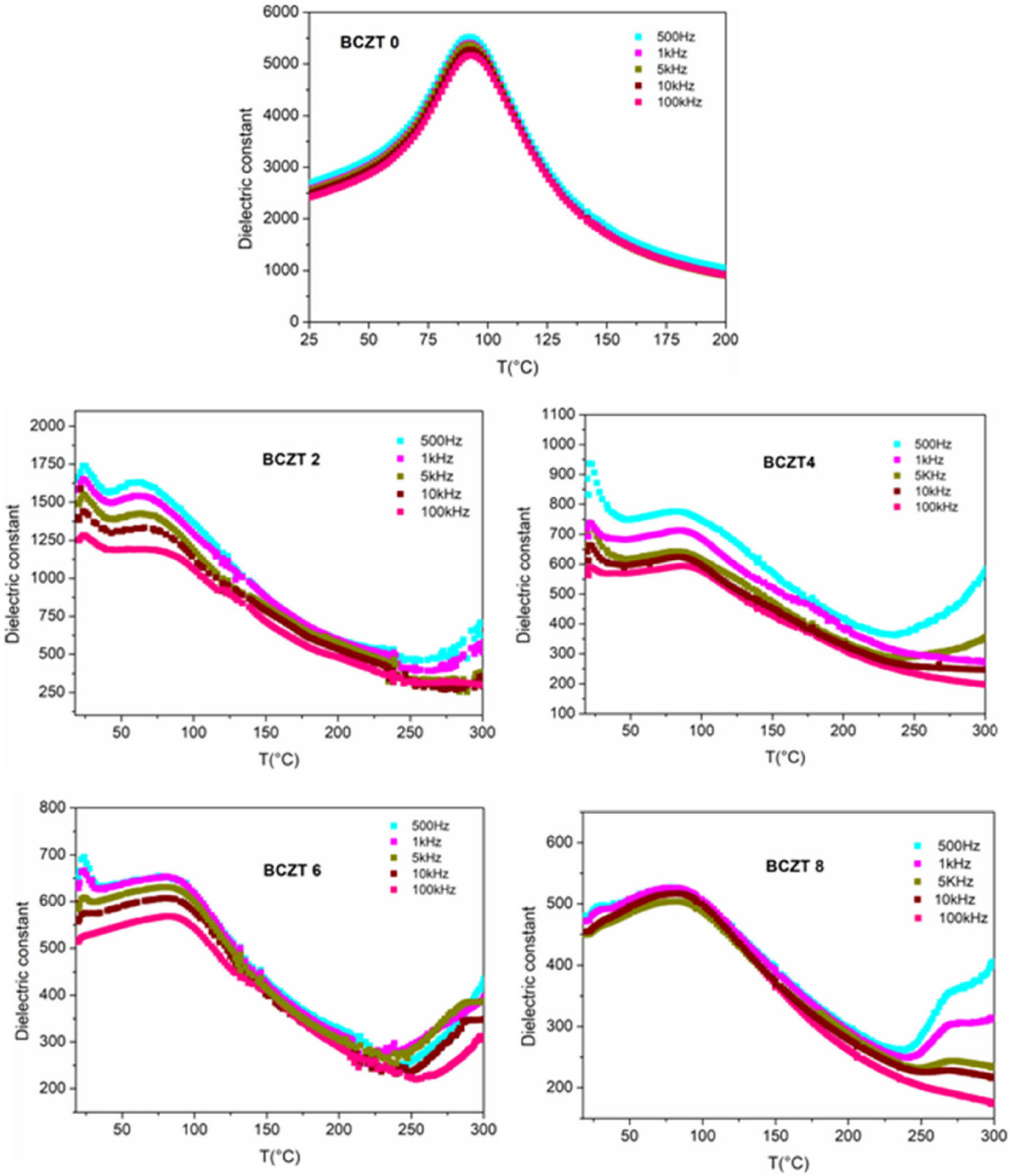

Fig. 4 Temperature dependence of ε_r of BCZTx ceramics at the frequency range of 500–100 kHz

The energy storage performances of BCZT*x* ceramics were determined from the recorded *P*–*E* hysteresis loops [26].

Figure 9 presents the evolution of W_{rec} and η as a function of the applied electric field for all the samples. It can be seen that W_{rec} of *BCZTx* ceramics increases as the applied electric field increases. This indicates that the increase of the applied external voltage can help to increase the recovered energy density. However, a significant decrease in energy efficiency was noted with this increase. This tendency could be linked to the greater energy loss caused by internal relaxation polarization in high electric fields. Pure BCZT ceramic has a low energy efficiency when compared to other ceramics. Nonetheless, adding the glass improves the energy efficiency (η) of *BCZTx* ceramics and keeps it at a higher level due to the reduction of energy loss. For instance, it increases

from 37% for BCZT0 to 66.7% and 62.4% for BCZT2 and BCZT4, respectively.

Figure 10 presents the variation of W_{loss}, W_{rec}, and η as a function of the glass content for all the samples at the maximum electric field. It is obvious that the energy density rises and subsequently drops as the percentage of glass increases. It increases form 0.075 to 0.506 J/cm^3, 0.521 J/cm^3, 0.0884 J/cm^3, and 0.0577 J/cm^3 for BCZT0, BCZT2, BCZT4, BCZT6, and BCZT8, respectively. The increase in W_{rec} is related to the increase in the maximum applied electric field. Likewise, it was enhanced substantially from 25 kV/cm for BCZT0 to 135 kV/cm for BCZT4, and then decreases. However, BCZT6 and BCZT8 ceramics display a relatively large maximum electric field, 62 kV/cm and 57 kV/cm, respectively, compared to pure BCZT ceramic. It is well known that a number of variables, including porosity, grain size, the second phase, sintering temperature, charge injection, and interfacial polarization, have a significant impact on the BDS of ceramics [36, 37]. By adding a glass, the liquid phase develops between the grain boundaries during the sintering of the ceramics, which favors the microstructure densification and restrains the grain

Table 1 The dielectric constant and the peak temperatures of the phase transitions of BCZTx ceramics

Sample	$T_{O\text{-}T}$ (°C)	ε_r (30 °C, 1 kHz)	T_c (°C)	ε_m (1 kHz)
BCZT0	35	2640	92	5400
BCZT2	24.7	1587	63	1542
BCZT4	22.3	692	86	710
BCZT6	23	630	84	651
BCZT8	29.5	488	80	524

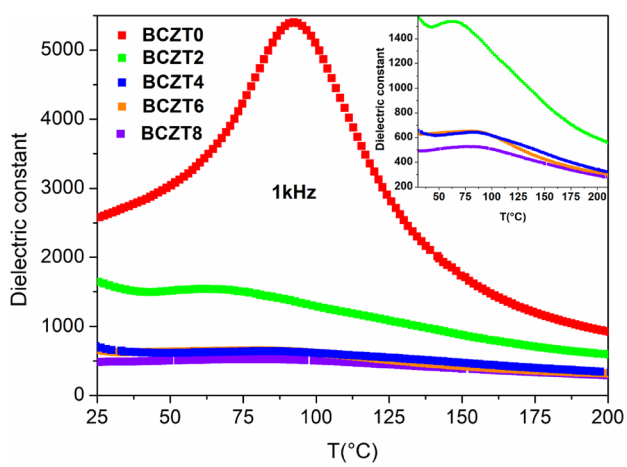

Fig. 5 Temperature dependence of ε_r of BCZTx ceramics at 1 kHz

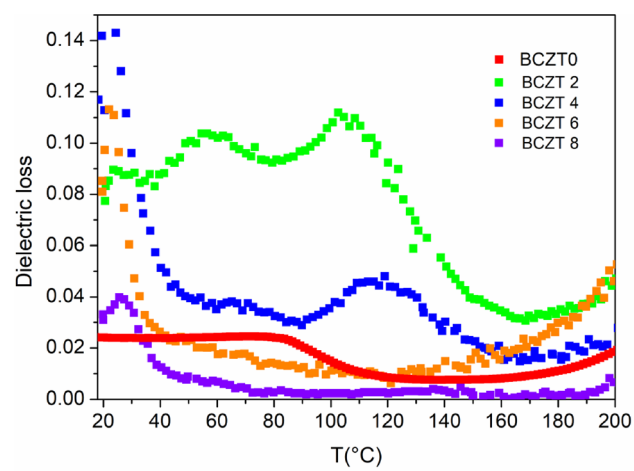

Fig. 6 Temperature dependence of *tanδ* of BCZTx ceramics at 1 kHz

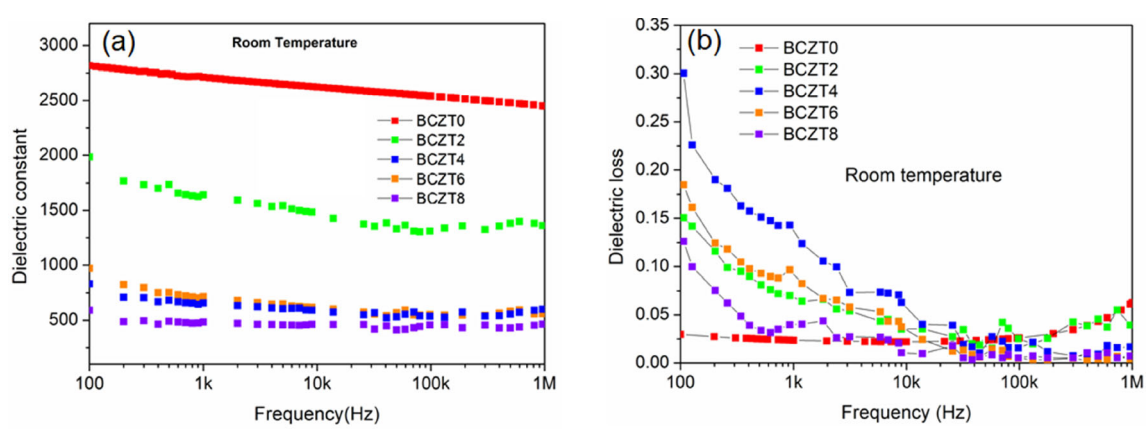

Fig. 7 Room temperature frequency dependence of **a** ε_r and **b** tan δ of BCZTx ceramics

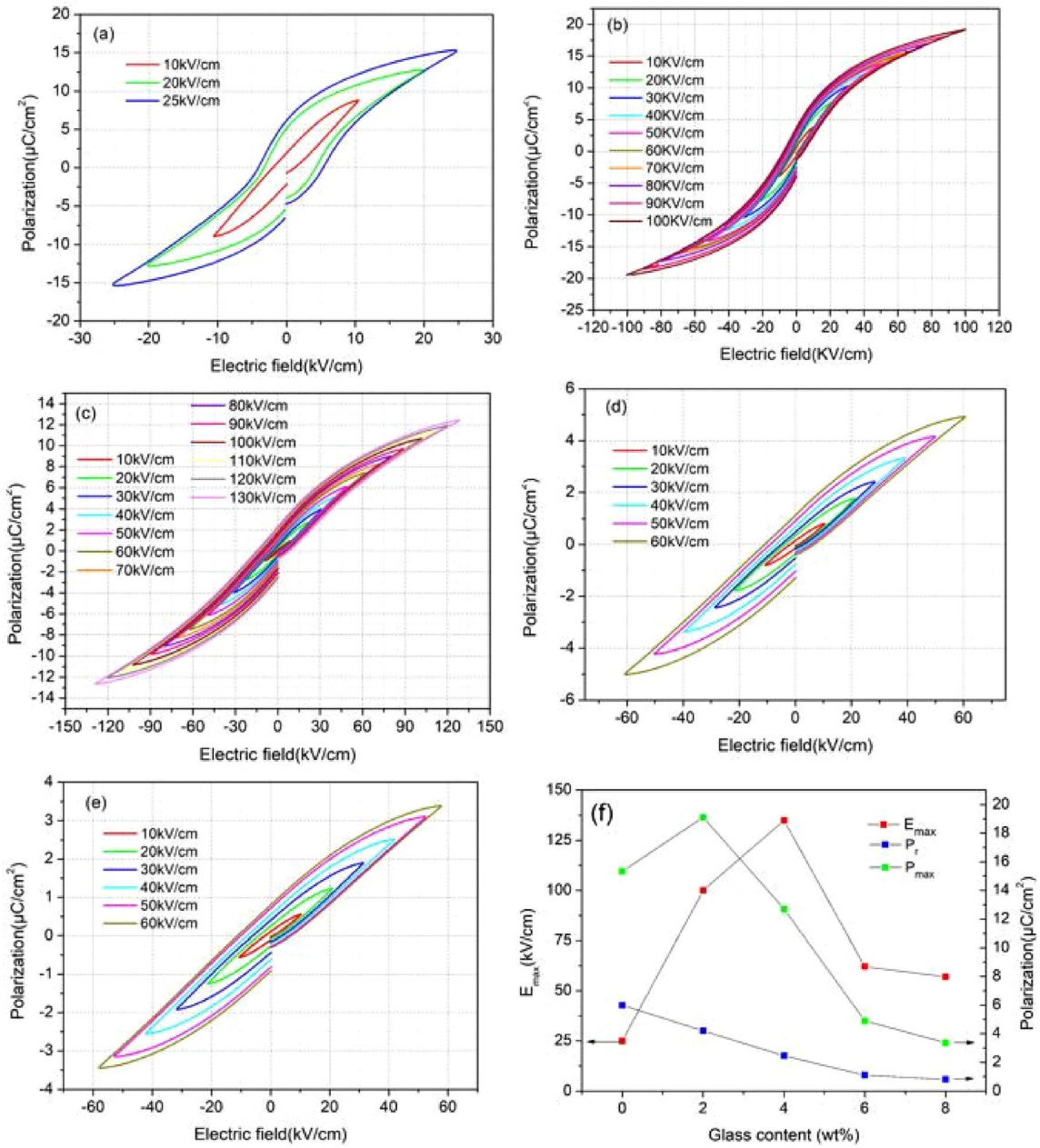

Fig. 8 **a**–**e** *P*–*E* hysteresis loops of BCZT*x* ceramics and **f** P_{max}, P_r, and E_{max} values of the BCZT*x* ceramics

overgrowth, leading to dense ceramics with higher BDS. The addition of glass to BCZT ceramics significantly refined the microstructure, as evidenced by the SEM images. Previous research has suggested that decreasing grain size improves *BDS*, as demonstrated by the relation,$E_{BDS} \propto G^{-c}$, where E_{BDS} is the breakdown strength, *G* is the average grain size, and *c* is a constant [38]. Furthermore, the glass-forming phase at the grain boundary can aid to enhance the BDS by preventing the grains from breaking at high-applied voltage. One can notice that the BDS differences between the samples are so large and significant. In fact, the BDS of BCZTx ceramics is suddenly dropped from 135 kV/cm (x = 4) to 60 kV/cm (x = 6). Meanwhile, the BDS of BCTZ0 ceramics is lower than 30 kV/cm. The enhancement of BDS was associated with the decrease of the grain, the improvement of homogeneous microstructure, and the improvement in the density of BCZTx ceramics. However, the decrease of BDS for BCZT4 and BCZT6

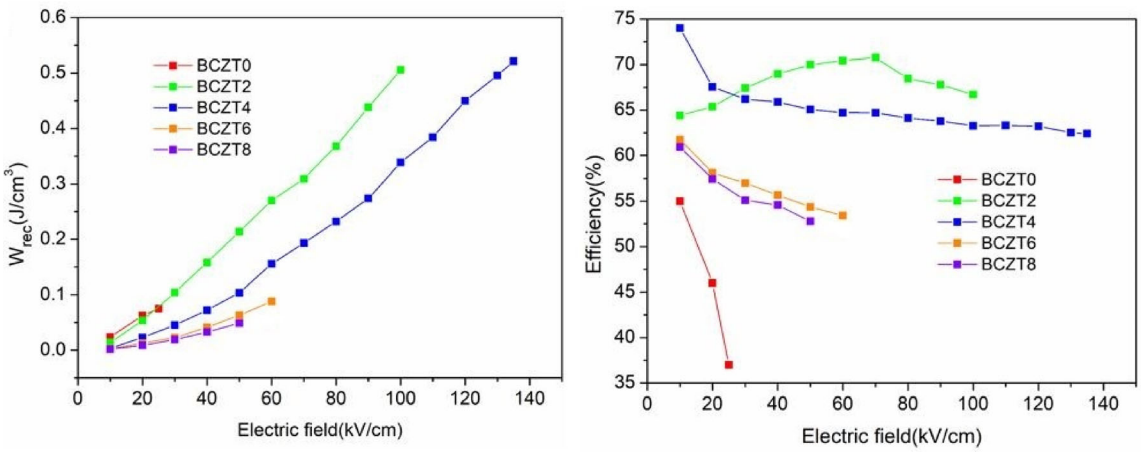

Fig. 9 Electric field dependence of **a** Wrec and **b** η for all the samples

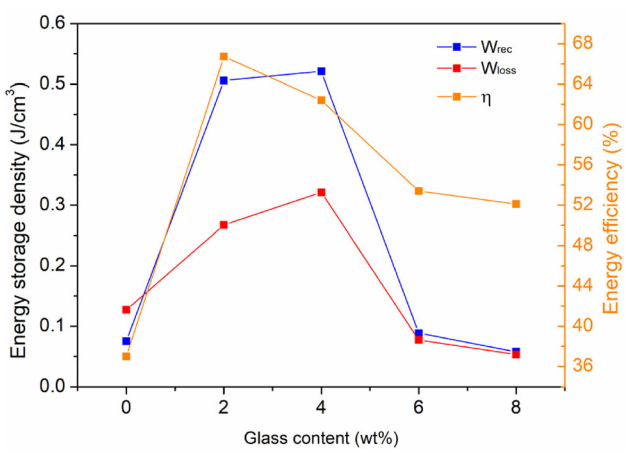

Fig. 10 Wtot, Wrec, and η of BCZTx ceramics with different glass additions

could be associated to the decrease of the density of samples and the formation of the impurity phase [39], which is evident from Figs. 1 and 3. Moreover, this degradation of BDS may be caused by the coarsening of glass and formation of discontinuous grain boundary precipitates in ceramics [35].

The optimum energy density is obtained for BCZT4 ceramic with the highest maximal electric field. It reaches 0.52 J/cm^3 at 135 kV/cm with an energy efficiency of ($\eta \sim 62.4\%$), which is multiplied by 6.6 compared to BCZT0 the BCZT0 ($W_{rec} \sim 0.075$ J/cm^3). As predicted, the addition of glass to BCZTx ceramics can considerably increase the energy efficiency and recoverable energy density.

Table 2 summarizes the ε_r, W_{tot}, W_{rec}, and η of other glass-modified lead-free ferroelectric ceramics and BCZTx samples at the high electric field. BCZT4 sample shows improved energy storage density than other ceramics at room temperature, [40, 41]. Note that a W_{rec} of 0.192 J/cm^3 with an η of 78% was achieved for $Ba(Zr_{0.2}Ti_{0.8})O_3$–0.15$(Ba_{0.7}\ Ca_{0.3})TiO_3$ ceramic [40]. Meanwhile, Wang et al.[22] reported a large W_{rec} of 2.12 J/cm^3 and high η of 90.5% in $Ba_{0.85}Ca_{0.15}Zr_{0.1}Ti_{0.9}O_3/Bi_2O_3$–$B_2O_3$–$SiO_2$ ceramic under an applied electric field of 330 kV/cm.

3.4.1 *Landau theory*

Based on the Landau–Ginzburg–Devonshire (LGD) phenomenological theory, more understanding of the calculations of the energy density parameters (W_{rec}, W_{tot}, η) can be obtained.

$$F = \frac{1}{2}aP^2 + \frac{1}{4}bP^4 - EP, \tag{1}$$

where a and b are quadratic and quartic factors, respectively.

In a state of equilibrium, $\frac{\partial F}{\partial P} = 0$, which results in

$$E = aP + bP^3. \tag{2}$$

The polarization dependence of electric field (E–P) data can be fitted by Eq. (2), showing the validity of the equation and enabling the extraction of the coefficients a and b for each sample. For instance, these latter a and b coefficients are shown in Fig. 11 for BCZT4 sample. According to the Landau model, these a and b parameters are significant for energy storage density [44] since they are involved in the following expression:

$$W = \int_0^{P_{max}} (aP + bP^3)dp = \frac{1}{2}aP_{max}^2 + \frac{1}{4}bP_{max}^4, \tag{3}$$

Table 2 Comparison of the dielectric constant and the energy storage properties of BCZT ceramic with other BT-based ceramics modified by glass addition reported in the literature

Samples	ε_r (30 °C, 1 kHz)	E_{max} (kV/cm)	W_{tot} (J/cm^3)	W_{rec} (J/cm^3)	η (%)	Ref
BCZT2	1587	100	0.758	0.506	66.7	This work
BCZT4	692	135	0.834	0.521	62.4	This work
$Ba(Zr_{0.2}Ti_{0.8})O_3$–0.15$(Ba_{0.7}Ca_{0.3})TiO_3$–BaO–SrO–TiO_2–Al_2O_3–SiO_2–BaF_2	500	96	0.192	0.149	~ 78	[40]
$Ba_{0.95}Sr_{0.05}Zr_{0.2}Ti_{0.8}O_3$–MgO–CaO–$Al_2O_3$–$SiO_2$	1000	140	0.5	0.42	82.8	[41]
$Ba_{0.4}Sr_{0.6}Zr_{0.15}Ti_{0.85}O_3$–SrO–$B_2O_3$–$SiO_2$	700	100	0.51	0.45	88.2	[42]
$Ba_{0.95}Ca_{0.05}Zr_{0.3}Ti_{0.7}O_3$–MgO–CaO–$Al_2O_3$– SiO_2	1420	140	0.63	0..49	77.0	[43]
$Ba_{0.85}Ca_{0.15}Zr_{0.1}Ti_{0.9}O_3$ + B_2O_3–Al_2O_3-SiO_2	950	200	1.53	1.15	75	[2]
$Ba_{0.85}Ca_{0.15}Zr_{0.1}Ti_{0.9}O_3$–$Bi_2O_3$–$B_2O_3$–$SiO_2$	895	330	2.34	2.12	90.5	[22]

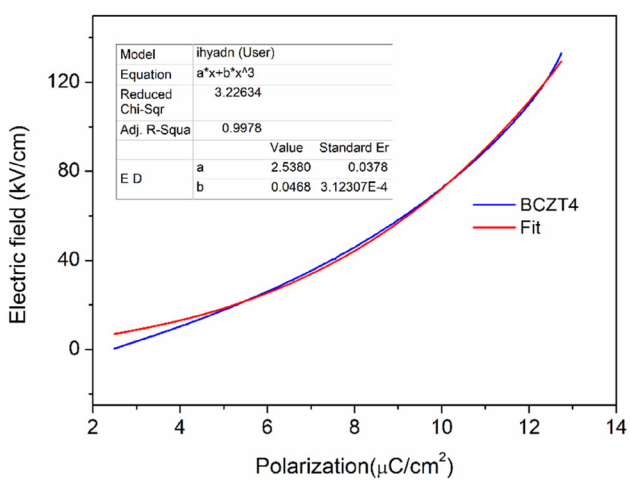

Fig. 11 *E–P* hysteresis curves and the fitting parameters (*a* and *b*) during the discharge processes of BCZT4 sample

where P_{max} is the polarization at E_{max} and a and b are constant values. Equation (6) therefore tells us that only three quantities completely govern the behaviors and values of the energy density, namely *a*, *b*, and P_{max}. Table 3 presents the parameter's *a* and *b* obtained and the experimental energy density (W_{rec} and W_{tot}) and theoretical energy density calculated using Eq. (3).

4 Conclusion

$Ba_{0.85}Ca_{0.15}Zr_{0.1}Ti_{0.9}O_3$ ceramics modified with the BaO–Na_2O–Nb_2O_5–WO_3–P_2O_5 glass addition were synthesized using the solid-state reaction technique. The inclusion of glass results in smaller grain sizes and a dense microstructure. The dielectric measurements showed that the dielectric constant decreased as the BNNWP glass content increases. Thin hysteresis loops with larger electric field were noticed for modified BCZT*x* ceramics. The maximal electric field of BCZT4 ceramic was remarkably improved for almost five times with respect to the pure BCZT ceramic. As a result, BCZT4 ceramic showed the highest recovered energy density of 0.52 J/cm^3 at 135 kV/cm with an energy efficiency of 62.4%. The calculated theoretical energy densities from the Landau–Ginzburg–Devonshire (LGD) theory are compatible with the experimental findings.

Table 3 The obtained parameters (a and b), the experimental and theoretical energy storage parameters (W_{rec},W_{tot}, and η)

Sample	$a_{(Wtot)}$	$b_{(Wtot)}$	$W_{tot(exp)}$	$W_{tot(th)}$	$W_{rec(exp)}$	$W_{rec(th)}$	η_{exp}	η_{exp}
BCZT0	1.3275	0.001448	0.202	0.173	0.75	0.70	37	40.3
BCZT2	2.65793	0.00681	0.758	0.721	0.50	0.492	66.72	68.2
BCZT4	8.95565	0.00878	0.803	0.782	0.52	0.512	62.4	65.47
BCZT6	14.51299	− 0.11058	0.165	0.160	0.84	0.917	53.4	57.3
BCZT8	20.78449	− 0.39079	0.110	0.106	0.577	0.587	52.14	55.42

Importantly, the theoretical energy density parameters (W_{rec}, W_{tot}, and η) calculated by the Landau theory are in agreement with the experimental results

Acknowledgements

The authors gratefully acknowledge the financial support of CNRST, OCP foundation, and the European Union's Horizon H2020-MSCA-RISE research and innovation actions, ENGIMA and MELON.

Author contribution

All authors certify that they have participated sufficiently in the work to take public responsibility for the content. Furthermore, each author certifies that this work will not be submitted to other journal or published in any other publication before. AI: Investigation, Writing—Original Draft, visualization, and conceptualization; SM: Writing—Review & Editing; DM: Conceptualization, validation, resources, and supervision; LB: Conceptualization, resources, and supervision; AL: Writing—Review and Editing; AA: Software and supervision; MA and IAL: Reviewing and Editing; MEM: Formal analysis and Resources.

Funding

CNRST Morocco, OCP foundation.

Data availability

Not applicable.

Code availability

Not applicable.

Declarations

Conflicts of interest Not applicable.

Ethical approval Not applicable.

Consent to participate We confirm that all authors mentioned in the manuscript have participated in, read and approved the manuscript, and have given their consent for the submission and subsequent publication of the manuscript.

Consent for publication We confirm that all the authors mentioned in the manuscript have agreed to publish this paper.

References

1. Z. Yao, Z. Song, H. Hao, Z. Yu, M. Cao, S. Zhang, M.T. Lanagan, H. Liu, Adv. Mater. (2017). https://doi.org/10.1002/adma.201601727
2. H. Yang, F. Yan, F. Wang, G. Zhang, Y. Lin, J. Alloys Compd. (2017). https://doi.org/10.1016/j.jallcom.2017.05.158
3. J. Liu, J. Zhai, K. Yang, B. Shen, S. Wang, J. Tian, Ceram. Int. (2018). https://doi.org/10.1016/j.ceramint.2018.02.054
4. X. Chen, Y. Tang, X. Bo, J. Song, J. Luo, J. Mater. Sci. Mater. Electron. (2018). https://doi.org/10.1007/s10854-018-9858-6
5. Z. Yang, H. Du, S. Qu, Y. Hou, H. Ma, J. Wang, J. Wang, X. Wei, Z. Xu, J. Mater. Chem. A (2016). https://doi.org/10.1039/c6ta04107h
6. D. Li, X. Zeng, Z. Li, Z.Y. Shen, H. Hao, W. Luo, X. Wang, F. Song, Z. Wang, Y. Li, J. Adv. Ceram. (2021). https://doi.org/10.1007/s40145-021-0500-3
7. X. Hao, J. Adv. Dielectr. (2013). https://doi.org/10.1039/c6ta04107h10.1142/s2010135x13300016
8. M. Zhang, H. Yang, Y. Lin, Q. Yuan, H. Du, Energy Storage Mater. (2022). https://doi.org/10.1016/j.ensm.2021.12.037
9. H. Yang, F. Yan, Y. Lin, T. Wang, J. Eur. Ceram. Soc. (2018). https://doi.org/10.1016/j.jeurceramsoc.2017.11.058

10. S. Merselmiz, Z. Hanani, D. Mezzane, M. Spreitzer, A. Bradeško, D. Fabijan, D. Vengust, M. Amjoud, L. Hajji, Z. Abkhar, A.G. Razumnaya, B. Rožič, I.A. Luk'yanchuk, Z. Kutnjak, Ceram Int Ceram Int (2020). https://doi.org/10.1016/j.ceramint.2020.06.16
11. Z. Hanani, S. Merselmiz, D. Mezzane, A. Bradeško, B. Rožič, M. Lahcini, M. El Marssi, A.V. Ragulya, I.A. Luk'Yanchuk, Z. Kutnjak, M. Gouné, RSC Adv (2020). https://doi.org/10.1039/d0ra06116f
12. S.S. Merselmiz, Z. Hanani, U. Prah, D. Mezzane, L. Hajji, Z. Abkhar, M. Spreitzer, D. Vengust, H. Uršič, D. Fabijan, A. Razumnaya, O.G. Shapovalova, I.A. Luk'yanchuk, Z. Kutnjak, Phys. Chem. Chem. Phys. (2022). https://doi.org/10.1039/D1CP04723J
13. Y. Lin, D. Li, M. Zhang, S. Zhan, Y. Yang, H. Yang, Q. Yuan, A.C.S. Appl, Mater. Interfaces. (2019). https://doi.org/10.1021/acsami.9b10819
14. Z. Hanani, D. Mezzane, M. Amjoud, S. Fourcade, A.G. Razumnaya, I.A. Luk'yanchuk, M. Gouné, Superlattices Microstruct. (2019). https://doi.org/10.1016/j.spmi.2018.03.004
15. H. Kaddoussi, A. Lahmar, Y. Gagou, B. Manoun, J.N. Chotard, J.-L. Dellis, Z. Kutnjak, H. Khemakhem, B. Elouadi, M. El Marssi, J. Alloys Compd. (2017). https://doi.org/10.1016/j.jallcom.2017.04.148
16. S. Merselmiz, Z. Hanani, D. Mezzane, A.G. Razumnaya, M. Amjoud, L. Hajji, S. Terenchuk, B. Rǒzic, I.A. Luk'yanchukc, Z. Kutnjak, RSC Adv (2021). https://doi.org/10.1039/d0ra09707a
17. Z. Dai, J. Xie, Z. Chen, S. Zhou, J. Liu, W. Liu, Z. Xi, X. Ren, Chem. Eng. J. (2020). https://doi.org/10.1016/j.cej.2020.128341
18. W.S.M. Maraj, W. Wei, B. Peng, Materials (Basel). (2019). https://doi.org/10.3390/ma12213641
19. Y. Lin, Y. Zhang, S. Zhan, C. Sun, G. Hu, H. Yang, Q. Yuan, J. Mater. Chem. A. (2020). https://doi.org/10.1039/D0TA07937E
20. T. Wu, Y. Pu, T. Zong, P. Gao, J. Alloys Compd. (2014). https://doi.org/10.1016/j.jallcom.2013.09.072
21. Z. Luo, L. Han, A. Lu, J. Song, Q. Feng, T. Liu, J. Mater. Sci. Mater. Electron. (2018). https://doi.org/10.1007/s10854-018-8566-6
22. X.W. Wang, B.H. Zhang, Y.C. Shi, Y.Y. Li, M. Manikandan, S.Y. Shang, J. Shang, Y.C. Hu, S.Q. Yin, J. Appl. Phys. (2020). https://doi.org/10.1063/1.5138948
23. V.S. Puli, A. Kumar, R.S. Katiyar, X. Su, C.M. Busta, D.B. Chrisey, M. Tomozawa, J. Non. Cryst. Solids. (2012). https://doi.org/10.1016/j.jnoncrysol.2012.05.018
24. A. Ihyadn, D. Mezzane, M. Amjoud, A. Lahmar, L. Bih, A. Alimoussa, I.A. Luk'Yanchuk, M. El Marssi, Today Proc (2022). https://doi.org/10.1016/j.matpr.2021.03.570
25. E. Haily, L. Bih et al., Mater. Chem. Phys. (2020). https://doi.org/10.1016/j.matchemphys.2019.122434
26. A. Ihyadn et al., Mater Res Express (2019). https://doi.org/10.1088/2053-1591/ab4569
27. Y. Yao, C. Zhou, D. Lv, D. Wang, H. Wu, Y. Yang, X. Ren, EPL (2012). https://doi.org/10.1209/0295-5075/98/27008
28. Z. Hanani, E.-H. Ablouh, M. Amjoud, D. Mezzane, M. Gouné, S. Fourcade, Ceram. Int. (2017). https://doi.org/10.1016/j.ceramint.2018.03.022
29. L.Z. Wang, W.Q. Luo, Z.M. Wang, Y.M. Li, Mater Electron J Mater Sci (2017). https://doi.org/10.1007/s10854-017-8010-3
30. W. Liu, W. Ping, S. Li, Energy Technol (2017). https://doi.org/10.1002/ente.201600713
31. Z. Yang, H. Du, L. Jin, D. Poelman, J. Mater. Chem. A (2021). https://doi.org/10.1039/d1ta04504k
32. Z.-Y. Shen, Y. Wang, Y. Tang, Y. Yu, W.-Q. Luo, X. Wang, Y. Li, Z. Wang, F. Song, J. Mater. (2019). https://doi.org/10.1016/j.jmat.2019.06.003
33. X. Du, Y. Pu, X. Li, X. Peng, Z. Sun, J. Zhang, J. Ji, R. Li, Q. Zhang, M. Chen, Ceram. Int. (2021). https://doi.org/10.1016/j.ceramint.2020.12.021
34. Z. Jiwei, Y. Xi, C. Xiaogang, Z. Liangying, H. Chen, Sci. Eng. B Solid-State Mater. Adv. Technol. Mater (2002). https://doi.org/10.1016/S0921-5107(02)00061-2
35. Y.H. Huang, Y.J. Wu, B. Liu, T. Yang, J. Wang, J. Li, L. Chen, X.M. Chen, J. Mater. Chem. A (2018). https://doi.org/10.1039/C7TA10821D
36. X. Wang, Y. Zhang, X. Song, Z. Yuan, T. Ma, Q. Zhang, C. Deng, T. Liang, J. European Ceramic Society. (2012). https://doi.org/10.1016/j.jeurceramsoc.2011.09.024
37. C. Liu, X. Chen, B. Zeng, F. Zhang, W. Song, Z. Luo, Y.L. Wang, J Adv Ceram (2023). https://doi.org/10.26599/JAC.2023.9220713
38. J. Wang, C. Xu, B. Shen, J. Zhai, J. Mater. Sci. Mater. Electron. (2013). https://doi.org/10.1007/s10854-013-1248-5
39. T. Wang, Y. Wang, H. Yangy, Y. Lin, L. Kong, J. Adv. Dielectr. (2018). https://doi.org/10.1142/S2010135X18500418
40. W. Liu, W. Ping, S. Li, Energy Technol. **5**, 1423–1428 (2017)
41. Q. Xu, D. Zhan, D.P. Huang, H.X. Liu, W. Chen, F. Zhang, J. Alloys Compd. (2013). https://doi.org/10.1016/j.jallcom.2012.12.164
42. T. Wu, Y. Pu, K. Chen, Ceram. Int. (2013). https://doi.org/10.1016/j.ceramint.2013.02.009

43. D. Zhan, Q. Xu, D.P. Huang, H.X. Liu, W. Chen, F. Zhang, Phys. B Condens. Matter. (2014). https://doi.org/10.1016/j.physb.2014.01.025
44. Z. Jiang, S. Prosandeev, L. Bellaiche, Phys. Rev. B. (2022). https://doi.org/10.1103/PhysRevB.105.024102